crystals

MDPI

Article

Design and Investigation of a Side-Chain Liquid Crystalline Polysiloxane with a N_{tb}-Phase-Forming Side Chain

Wanhe Jiang and Georg H. Mehl *

Department of Chemistry, University of Hull, Hull HU6 7RX, UK; w.jiang-2019@hull.ac.uk
* Correspondence: g.h.mehl@hull.ac.uk

Abstract: A new mesogenic non-symmetric dimeric monomer with a terminal olefin function, forming a twist bend nematic (N_{tb}) as well as a nematic (N) phase, was synthesized, using an enhanced synthetic methodology, which avoids isomerization of the terminal double bond in the preparation of the dimer. This monomer was attached to a pentamethyldisiloxane group, resulting in the SmA LC phase behavior of the ensuing material. Linking the monomer to a siloxane main chain resulted in nematic phase behavior. Detailed studies with the N_{tb} phase forming dimer DTC5C7 show full miscibility of the dimer and the new LC polymer in the LC state, suggesting that the side-chain LC polymer forms a N_{tb} phase as the low-temperature nematic phase. Copolymerizing the monomer with a cyanobiphenyl-based monomer allows us to tune the glass transition and phase behavior further.

Keywords: side-chain liquid crystal polymer; pentamethydisiloxane; N_{tb} phase; non-symmetric dimer; liquid crystal monomers; N_{tb} polymer

1. Introduction

Since the first side-chain liquid crystal polymer was reported in 1978 [1–6], the interest in the synthesis and applications of side-chain liquid crystal polymers (SCLCPs) has evolved. Side-chain liquid crystal polymers are polymers where mesogenic units are attached to backbones via flexible spacers. Thus, three elements are crucial in determining the properties of liquid crystal side-chain polymers: the polymer backbones, the spacers and the mesogenic units. Among all the backbones reported in the literature, polymethylsiloxanes are arguably the most flexible; this is combined with their excellent thermal stability and low glass transition temperatures. For a given backbone, the molecular structure of the mesogenic units, together with the length and parity of spacers, can have a profound effect on liquid crystal properties and the transition temperature ranges. However, as crystallization might be observed in some of the SCLCPs, a considerable amount of effort has been carried out to prevent polymers from unwanted crystallization and to reduce glass transition temperatures. Examples of such efforts are the use of different types of spacers [7], the variation of the length of the spacers [8] and the use of mesogens that are either terminally or laterally attached to the side chains [9]. Other tools are the use of copolymers with different mesogenic units [10] or even simply the use of non-mesogenic groups [11,12].

So far, there are no reports, to the best of our knowledge on polysiloxanes coupled with side-chain dimers to form side-chain liquid crystal polymers that exhibit N_{tb} phase behavior. Though it is noted that a number of polymers have been reported that carry di-mesogenic side chains, mainly based on malonate branching groups [13–15]. The N_{tb} phase for dimers is known to show often non-typical optical defect textures; also, it is not easy to distinguish the N_{tb} from the nematic phase by X-ray diffraction. So, in this study, a monomer was designed to consist of hydrocarbon units as spacers and terphenyl and biphenyl groups as mesogenic units, together with terminal double bonds, all designed for controlling the transition temperature and phase sequence. The overall approach is outlined schematically in Figure 1.

check for updates

Citation: Jiang, W.; Mehl, G.H. Design and Investigation of a Side-Chain Liquid Crystalline Polysiloxane with a N_{tb}-Phase-Forming Side Chain. *Crystals* **2023**, *13*, 1614. https://doi.org/10.3390/cryst13121614

Academic Editor: Borislav Angelov

Received: 26 October 2023
Revised: 15 November 2023
Accepted: 18 November 2023
Published: 21 November 2023

Copyright: © 2023 by the authors. Licensee MDPI, Basel, Switzerland. This article is an open access article distributed under the terms and conditions of the Creative Commons Attribution (CC BY) license (https://creativecommons.org/licenses/by/4.0/).

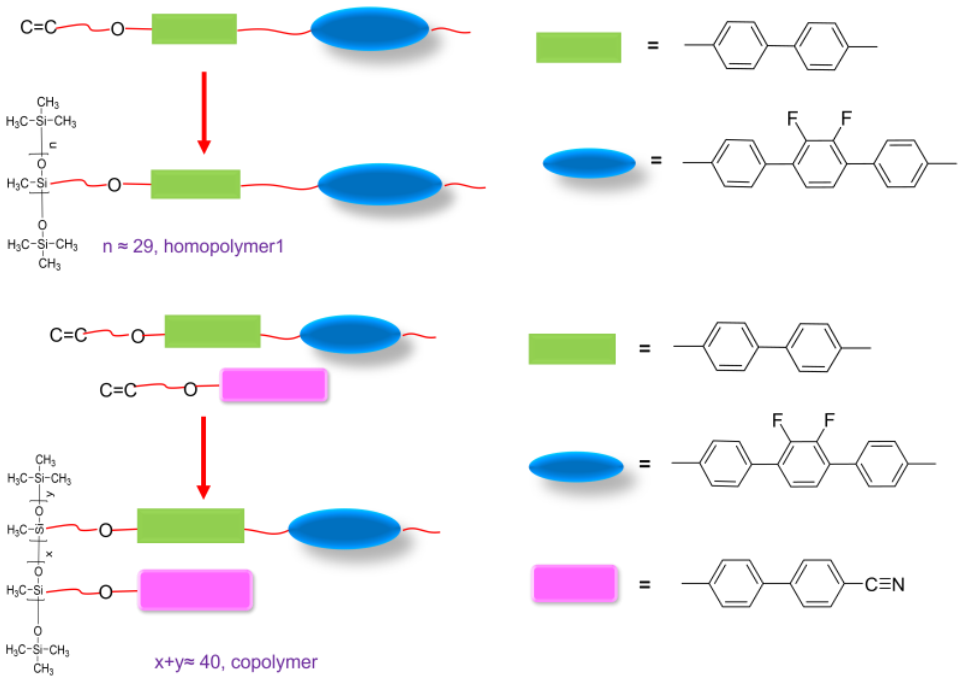


Figure 1. Schematic representation of the design approach for the LC polysiloxanes. The colored shapes represent the mesogenic units which have been employed.

The reason why this architecture was chosen is that: (a) it has been reported that dimers with similar structures such as **DTC5C$_n$** show the N_{tb} phase, even for related linear oligomers [16]. (b) The dimers structurally related to the system discussed here exhibit the N_{tb} phase over a large temperature range, a feature that makes it possible to tune the transition temperature of the N_{tb} phase by fine tuning the architecture [17]. Also, (c) a non-symmetric mesogenic system containing altogether five aromatic rings may result in a lower melting point when compared with a six-membered ring system. This is critical, as the transition temperatures of side-chain polymers are often higher than those of the monomers. Since pentamethydisiloxane derivatives can exhibit properties associated with polymers and maintain the low viscosity of monomers, it is interesting to investigate the liquid crystal functionalized N_{tb} system too. Additional results of a copolymerization that was carried out to eliminate crystallization are also reported. The overall approach is shown in Figure 1.

There were two challenges in this project. Firstly, there was a challenge in the preparation of the mesogen. The challenge was that isomers were formed. They are a byproduct of the Suzuki–Miyaura coupling reaction in the presence of hydrocarbon chains that carry olefinic functions. To eliminate the isomers, a co-catalyst was used together with the conventional Pd catalyst. The second challenge was that it was difficult to identify the N_{tb} phase of polymers; therefore, binary mixtures of the homopolymer with the N_{tb}-forming material were used to observe the liquid crystal defect textures using optical polarizing microscopy at controlled temperatures. The textures of the liquid crystal phases of the monomer and homopolymer 1 (**HP1**) were analyzed by polarized optical microscopy (POM) and differential scanning calorimetry (DSC) and through the construction of phase diagrams.

2. Experiment

2.1. Materials

Poly(methylhydrosiloxane) (average Mn 1700–3200) and a solution of platinum divinyl tetramethyl disiloxane complexes, with a platinum concentration of 2.5–5 wt%, were purchased from Sigma-Aldrich and used as received.

All other starting materials came from Sigma-Aldrich, Alfa Aesar, Manchester Organics, Fluorochem, TCI, ACROS organics and Apollo Scientific. All the company information is listed in the following: Apollo Scientific—Whitefield Rd, Bredbury, Stockport, SK6 2QR, UK; Sigma-Aldrich-Co., 3050 Spruce Street, St. Louis, MO 63103, USA; Tokyo Chemical Industry Co., Ltd. 6-15-9 Toshima, Kita-ku, Tokyo, Japan; ACROS organics-New Jersey, ISA 1-800-ACROS-01, Ceel, Belgium; Fluo-rochem-Fluorochem Ltd., Unit,14, Graphite Way, Hadfield, SK13, 1QH, UK; Alfa Ae-sar-Shore Road, Heysham, LA32XY, England; Manchester Organics-The Heath Business &Technical Park, Runcorn, Cheshire, UK, WA7 4QK. All compounds purchased were used without further purification. Silica gel 60 F254 Merck KGaA was used for thin-layer chro-matography.

The degree of polymerization written as $\overline{DP}$ is calculated by $\overline{Mw}/M_0$, using the values obtained by gel permeation chromatography (GPC), where Mw is the weight average molecular weight of the polymer, and M_0 is the molecular weight of the repeating unit of the monomer. The molecular weight distribution, also called polydispersity, is calculated by gel permeation chromatography (GPC) as the value of $\overline{Mw}/\overline{Mn}$.

2.2. Methods

Column chromatography: All purification by column chromatography utilized Fluorochem Ltd. Silica gel 60A 35–70-micron silica gel and Fisher Scientific Ltd. UK general purpose low iron grade sand. Company information in detail: Fisher scientific UK, Bishop Meadow Road, Loughbor-ough, Leics, LE11 5RG, UK.

^{1}H-NMR 400MHz, ^{13}C-NMR 101 MHz and ^{19}F-NMR 377 MHz were recorded on a Jeol JNM ECP400 spectrometer.

The thermal transitions were investigated by both differential scanning calorimetry (DSC) and polarized optical microscopy (POM). POM was performed using an Olympus BX51 Polarizing Microscope equipped with a Linkam LTS350 heating stage. The DSC data were from a Perkin Elmer Differential Scanning Calorimeter DSC 4000, an aluminum reference pan was used to load the reference and sample, and the calibration materials were standard indium. DSC results were normally quoted by the average values for the onset of the second heating and cooling curve. The heating rate, if not mentioned specifically, was at 10 °C/min.

Gel permeation chromatography (GPC) was run on a 350A HT-GPC system, equipped with two VE-1122 solvent delivery pumps, a VE-7510 solvent degasser, a Vortex 430 autosampler and the 350A HT detector module. The GPC is from Malvern Instruments, company detail as following: Malvern Instruments Ltd. Enigma Business Park, Grovewood Road, Malvern, Worcestershire WR14 1XZ, United Kingdom. Samples were passed through microfilters before measurement to remove the gel. Disposable microfilters were from Whatman Puradisc 25 TF. 0.2 μm PTFE Membrane with Polypropylene Housing Diameter 25 mm.

Elemental analysis was performed using FISONS Instruments EA 1108 CHN and using software Eager Xperience OS Version: 6.01 for processing the data.

X-ray powder diffraction data were collected from samples mounted on zero-background silicon discs. A PANAlytical Empyrean diffractometer operating in Bragg–Brentano geometry with copper Kα1 (λ = 1.541 Å) and a PIXEL detector was used for the data collection. Data were collected in the range $3^\circ \leq 2\theta \leq 30^\circ$.

Monomers were characterized by high-resolution mass spectrometers. The samples were run on the Bruker maXis, a Hybrid Quadrupole/Atmospheric Pressure Ionization orthogonal accelerated Time-Of-Flight mass spectrometer.

The side chain liquid crystal polymers were characterized by NMR, gel permeation chromatography (GPC), differential scanning calorimetry and optical polarizing microscopy.

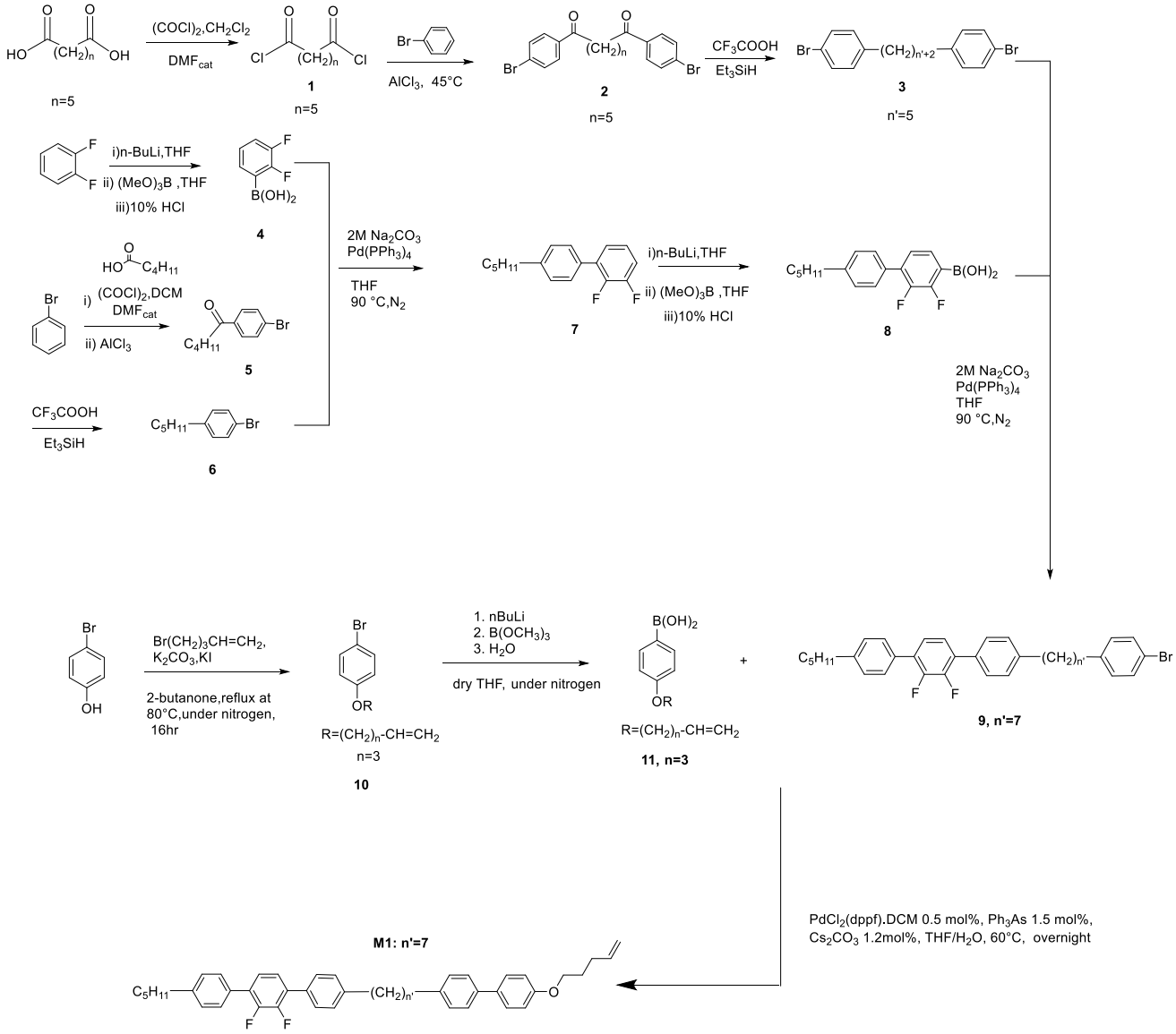
2.3. Purification of Polymers

As the amount of the monomers is always in excess in the polymer analogous reaction with the poly(methylhydro)siloxane backbone, and as the traces of monomers can

strongly influence the phase transition of related polymers, it was necessary to remove the monomers and purify the polymers. Purification was achieved by repeated precipitation with methanol, after dissolving the polymer with minimum volumes of toluene. The removal of monomers was monitored by DOSY-NMR and thin-layer chromatography on silica with an appropriate solvent combination.

2.4. Synthesis of Monomers

The synthesis route used to prepare the vinylic monomer is shown in Scheme 1. The monomer was synthesized in a twelve-step synthesis route, which was followed by the synthesis of the pentamethyldisiloxane derivative and the polymers.



Scheme 1. Synthesis route to monomer **M1**.

The overall synthesis is based on a convergent approach. It starts with the conversion of heptanedioic acid to the related acid chloride **1** by using oxalyl chloride. The acid chloride reacts with bromobenzene through a Friedel–Crafts acylation reaction to obtain compound **2**. The two keto groups were then reduced by a reaction with triethyl silane and trifluoroacetic acid to reach compound **3**. Compound **3** was reacted with compound **8**, which was obtained in a separate reaction pathway published earlier [17]. To make

compound **8**, the synthesis was based on another convergent synthesis route. After the reaction of 1,2-difluorobenzene with n-butyllithium, followed by a reaction with trimethyl borate, the boronic acid intermediate **4** was obtained. This was reacted in a coupling reaction with compound **6**. Compound **6** was obtained by reacting bromobenzene with oxalyl chloride and n-pentanoic acid in a Friedel–Crafts acylation, followed by the reduction of the ketone group with triethylsilane and trifluoroacetic acid. The coupling of compound **4** and compound **6** resulted in compound **7**, which was converted into a boronic acid by reacting first with n-butyllithium. This was followed by the reaction with trimethyl borate to form compound **8**. Compound **3** and compound **8** were coupled to form compound **9**. (shown in Scheme 1). The overall reaction pathway procedure toward this type of dimer has already been reported earlier, and hence the chemical characterization will not be reported here again [17].

Monomer **M1** was synthesized through a Suzuki–Miyaura coupling reaction of compound **9** and compound **11**. Compound **11** was prepared by a Williamson etherification, followed by lithiation and a Miyaura coupling reaction.

In this synthesis, for the preparation of the monomer, a cocatalyst was used in the Suzuki–Miyaura coupling to eliminate the formation of isomers in the alkene chain of the hydrocarbon groups of the monomers. The occurrence of isomerization reactions has been discussed early on, in 1993 [18]. An alternative to produce isomer-free products is to use $P(Ph_3)_4$ without a cocatalyst. It was found that the main catalyst concentration cannot be higher than 0.5% mol to avoid isomerization of the terminal double bond (see Figure 2b). However, in this procedure, the yield was only 15%, which is very low. Hence, a [1,1′-Bis(diphenylphosphino)ferrocene] dichloropalladium (II) complex with a dichloromethane/triphenyl arsine catalyst system was employed. The latter catalyst system was not only used to avoid formation of the isomers during the coupling reaction but also to help to maintain the yield of the isolated product after column chromatography at higher than 50%. This is due to the bulky structure of the main catalyst formed together with the cocatalyst, suppressing the beta-hydride elimination reaction which produces isomers. ^{1}HNMR results for the pure monomer are shown in Figure 2a, and an example of an isomer formed during the initial exploratory work is shown in Figure 2b.

The ^{1}HNMR ($CDCl_3$) spectra for **HP1** are virtually identical to the monomer **M1**, with the addition of the signals for the silyl protons at δ = 0.07 (48, s, Si-C$\underline{H}_3$) and δ= 0.86 (14,s, Si-C$\underline{H}_2$) and the loss of signals for the vinylic protons at δ = 5.99–5.75 (1H, m, -C$\underline{H}$ = CH_2) and 5.15–4.95 (2H, m, -CH = C$\underline{H}_2$). See below in Figures 2a and 3 as the ^{1}HNMR of monomer **M1** and polymer **HP1** separately. As typical for polymers, the signals are somewhat broader when compared to the monomer. The synthesis of monomer 4′-(pent-4-en-1-yloxy)-[1,1′-biphenyl]-4-carbonitrile discussed later in this work and corresponding homopolymer has been reported in detail much earlier [19,20].

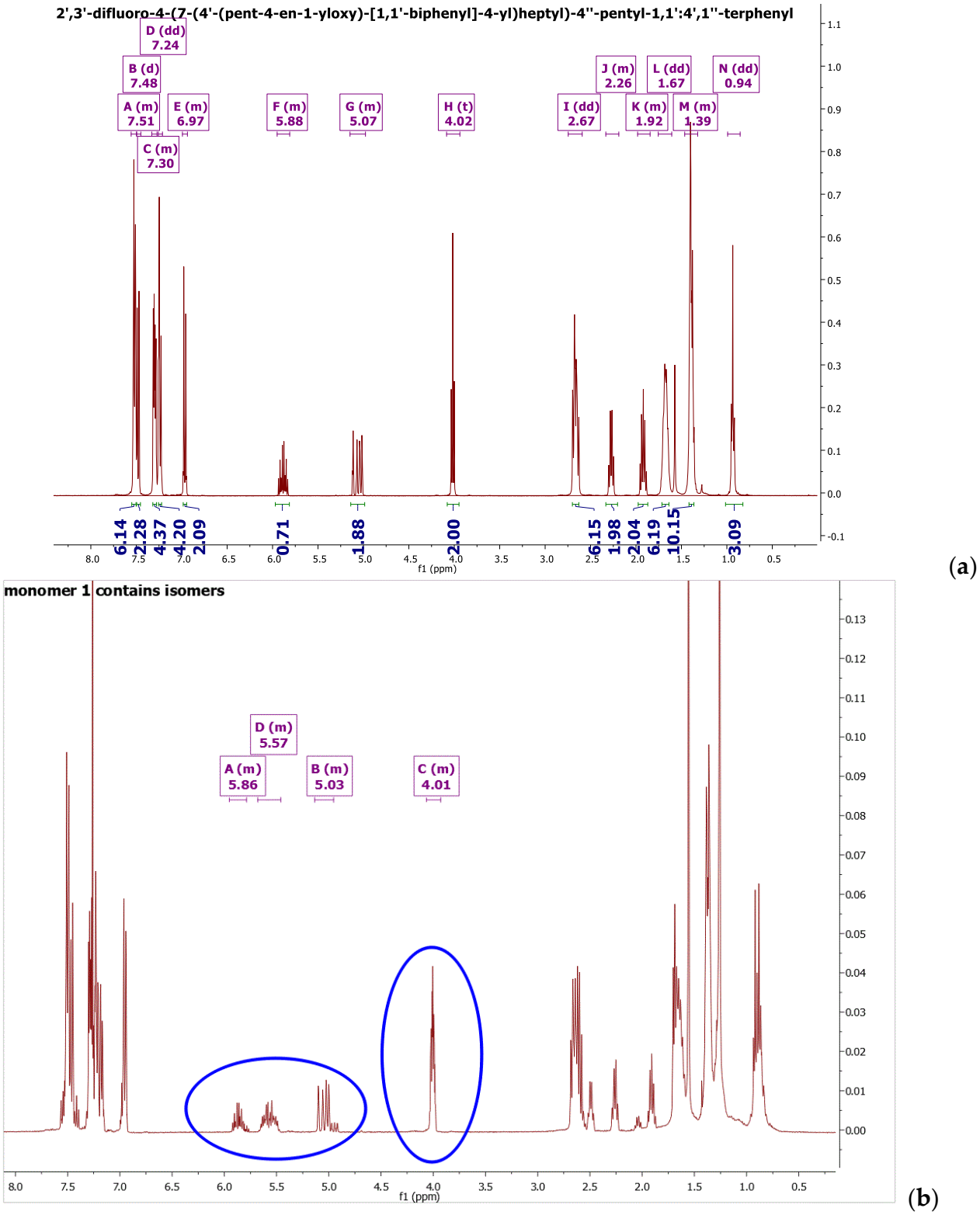


Figure 2. (**a**) ^{1}HNMR of pure monomer **M1**; (**b**) ^{1}HNMR of monomer **M1** with isomers (isomer peaks highlighted in a blue circle).

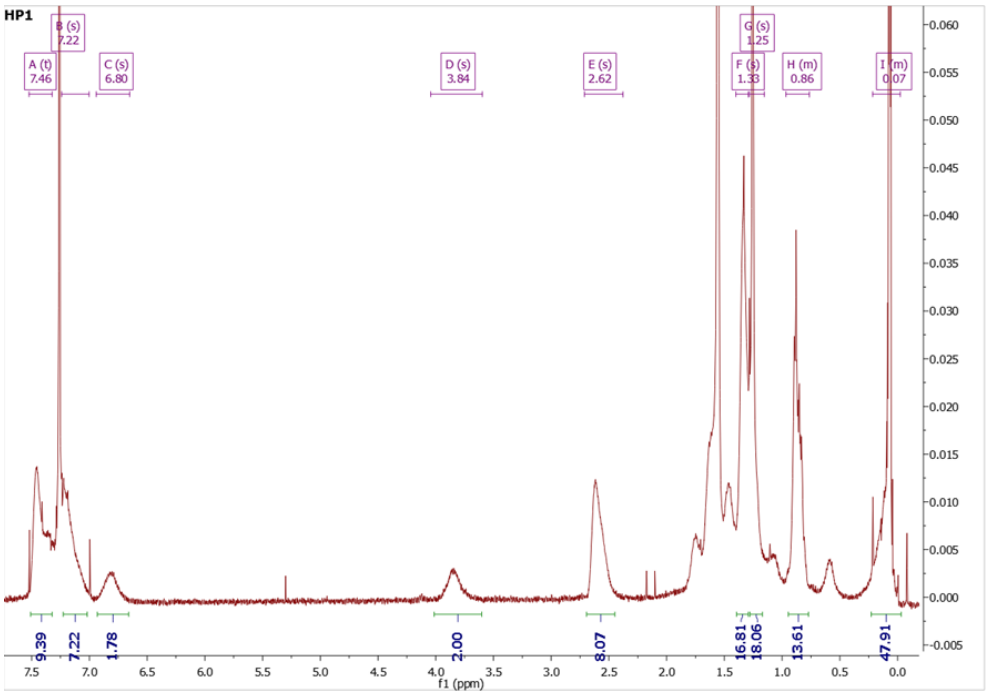


Figure 3. HNMR of homopolymer **HP1**.

Synthesis of the yet unreported steps for the preparation of **M1**.

2′3′-difluoro-4-(7-(4′-(pent-4-en-1-yloxy)-[1,1′-biphenyl]-4-yl)heptyl)-4″-pentyl-1,1′:4′,1″-terphenyl **M1**.

(2,3-difluoro-4-(pent-4-en-1-yloxy) phenyl) boronic acid **11** (0.11 g, 0.52 mmol) and 4-(7-(4-bromophenyl) heptyl)-2′,3′-difluoro-4″-pentyl-1,1′:4′,1″-terphenyl **9** (0.32 g, 0.52 mmol). Caesium carbonate was put in THF (50 mL) and water, and the solution was degassed 3 times. After that, the [1,1′-Bis(diphenylphosphino)ferrocene] dichloropalladium(II) complex with dichloromethane (2.12 mg, 0.5 mol%, 2.6×10^{-6} mmol) was added. This was followed by the addition of triphenyl arsine (23 mg, 1.5 mol% and 7.8×10^{-5} mmol), and the mixture was stirred at 60 °C overnight. The cooled mixture was poured into brine, and the product was extracted into chloroform (3×30 mL). The combined organic layer was dried by anhydrous $MgSO_4$, and the solvent was removed under vacuum. The crude compound **M1** was purified by column chromatography (DCM:Hexane = 1:4) and recrystallized from iso-propanol.

Yield: 0.18 g, 51.6%.

High-resolution mass spectroscopy: m/z 693.3883, err −0.4 ppm.

Elemental analysis: theoretical: C 84.14%; H 7.81%; experimental: C 84.20%; H 7.83%

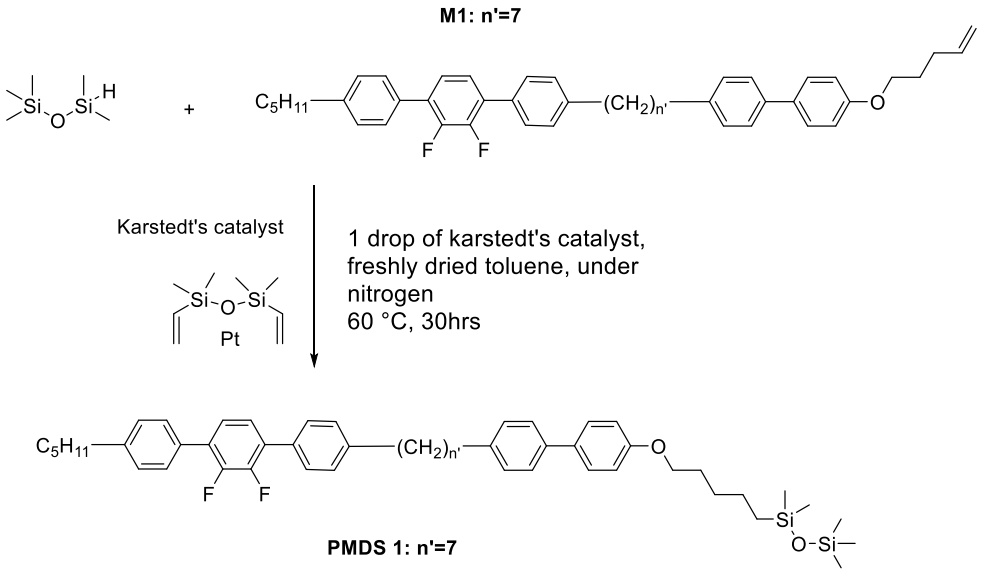
^{1}HNMR (400 MHz, $CDCl_3$): δ 7.56 – 7.50 (6H, m), 7.48 (2H, d, *J* = 8.1 Hz), 7.33 – 7.27 (4H,m), 7.24 (4H, dd, *J* = 6.2, 4.5 Hz), 6.99 – 6.94 (2H, m), 5.95 – 5.81 (1H,m), 5.15 – 4.98 (2H,m), 4.02 (2H, t, *J* = 6.5 Hz), 2.67 (6H, dd, *J* = 17.4, 9.8 Hz), 2.33 – 2.19 (2H, m), 1.98 – 1.84 (2H, m), 1.67 (6H, dd, *J* = 13.0, 6.8 Hz), 1.46 – 1.32 (10H, m), 0.94 (3H, dd, *J* = 9.0, 4.7 Hz).

^{13}CNMR (101 MHz, $CDCl_3$): δ 158.53, 143.23, 143.15, 141.52, 138.34, 137.98, 133.75, 132.04, 129.61, 128.91,128.82, 128.07, 126.69, 124.73, 124.70,115.34, 114.86, 67.37, 35.84, 35.68, 31.71, 31.61, 31.49, 31.25, 30.28, 29.48, 29.36, 28.61, 22.71, 14.20.

^{19}F NMR (377 MHz, $CDCl_3$): δ −143.21.

2.5. Synthesis of the Pentamethyldisiloxane Derivative (PMDS1)

The pentamethydisiloxane derivative was prepared by a platinum-catalyzed hydrosilylation, as shown in Scheme 2.



Scheme 2. Synthesis route of pentamethydisiloxane **PMDS 1**.

After the hydrosilylation reaction with 1,1,1,3,3-pentamethyl-1,3-disiloxane and **M1**, using Karstedt's catalyst, the pentamethydisiloxane derivative **PMDS1** was obtained (see Scheme 2). The synthesis is described in detail below:

1-(5-((4′-(7-(2′,3′-difluoro-4″-pentyl-[1,1′:4′,1″-terphenyl]-4-yl)heptyl)-[1,1′-biphenyl]-4-yl) oxy) pentyl)-1,1,3,3,3-pentamethyldisiloxane **PMDS 1**.

Monomer 2′,3′-difluoro-4-(7-(4′-(pent-4-en-1-yloxy)-[1,1′-biphenyl]-4-yl)heptyl)-4″-pentyl-1,1′:4′,1″-terphenyl **M1** (0.17 g, 0.254 mmol) in anhydrous toluene (50 mL) was stirred vigorously under nitrogen with 1,1,1,3,3-pentamethyldisiloxane (0.5 mL, 2.56 mmol) at 50 °C for 3 days, using a Karstedt's catalyst solution in xylene (Pt ~2%) (0.5 mL, 0.0224 mmol) as the catalyst. The solvent was removed by vacuum, and the catalyst was removed by passing the dry crude through silica gel and washing it with DCM. Silica gel column chromatography was used to further purify the crude (DCM/Petrol = 1/2). After recrystallization by isopropanol, it was obtained as a white solid, yielding 67 mg, 32.4%.

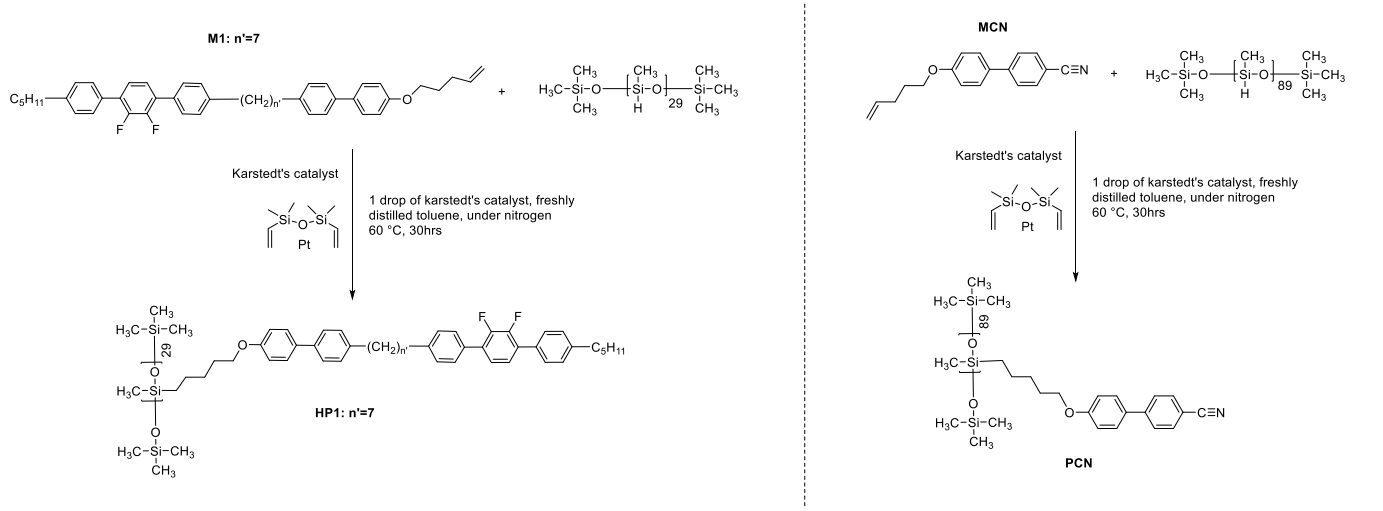
^{1}H NMR (400 MHz, $CDCl_3$): δ 7.54–7.43 (m, 8H), 7.32–7.26 (m, 4H), 7.23 (dd, J = 7.8, 5.0 Hz, 4H), 6.98–6.91 (m, 2H), 3.99 (t, J = 6.6 Hz, 2H), 2.65 (dt, J = 12.6, 8.0 Hz, 6H), 1.87–1.75 (m, 1H), 1.66 (dd, J = 13.0, 7.2 Hz, 6H), 1.45–1.19 (m, 17H), 0.99–0.81 (m, 6H), 0.10–0.03 (m,12H).

(Carbon-fluorine-proton decoupled) ^{13}CNMR (101 MHZ, $CDCl_3$): δ 158.63, 148.63, 143.20, 143.12, 141.39, 138.36, 133.60, 132.11, 129.60, 128.89, 128.85, 128.81, 128.03, 126.66, 124.68, 114.83, 68.16, 35.83, 35.68, 31.71, 31.61, 31.49, 31.25, 29.88, 29.49, 29.21, 28.37, 23.29, 22.71, 22.64, 18.46, 14.20, 2.14, 1.18, 0.51.

^{19}FNMR (376 MHz, $CDCl_3$): δ −143.12.

2.6. Synthesis of the Homopolymers (HP1 and PCN)

After a hydrosilylation reaction with poly(methylhydrosiloxane) and **M1**, using Karstedt's catalyst, **HP 1** and **PCN** were obtained. The synthesis is described in detail below (see Scheme 3).



Scheme 3. Synthesis route of homopolymer **HP1** and **PCN**. **PCN** has been previously reported [21,22].

2.6.1. **PCN**

PCN has been reported earlier [21,22]. The phase transition was found to be I-Sm_A 166.6 °C in this work, a value that is very close to the transition temperature reported previously of I-Sm_A 169.5 °C [21,22].

The polymer was synthesized by a hydrosilylation reaction of the monomer 4′-(pent-4-en-1-yloxy)-[1,1′-biphenyl]-4-carbonitrile (1.2 g, 4.56 mmol) and polymethylhydrosilane (Mn ≈ 1700~3200, 0.228 g, 3.8 mmol) using dry toluene as solvent with 2 drops of Karsted's catalyst (Pt ~2%), and the solution was stirred at 60 °C for 3 days whilst under an atmosphere of nitrogen. After the reaction was completed, further purification was carried out by repeated precipitation into methanol several times, and the product was dried under vacuum.

Isolated yield: 0.25 g, 20.4%.

^{1}H-NMR (400 MHz, $CDCl_3$): δ 7.47 (s, 14H), 7.25–7.00 (m, 8H), 6.84 (s, 4H), 3.86 (s, 4H), 2.63 (s, 7H), 1.61 (t, 26H), 0.90 (s, 4H), 0.59 (s, 4H), 0.09 (d, 19H).

The calculation of the yield is listed in Figure S1.

2.6.2. **HP1**

2′,3′-difluoro-4-(7-(4′-(pent-4-en-1-yloxy)-[1,1′-biphenyl]-4-yl)heptyl)-4″-pentyl-1,1′:4′,1″-terphenyl **M1** (0.15g, 0.224 mmol) in dry toluene (30 mL) was stirred with polymethylhydrosilane (Mn ≈ 1700~3200, 0.01g, 0.166 mmol) at 60 °C under nitrogen, and then 1 drop of Karsted's catalyst (Pt ~2%) was added. The reaction mixture was stirred for 3 days. After the reaction finished, purification was carried out by repeated precipitations into methanol, and the product was dried under vacuum.

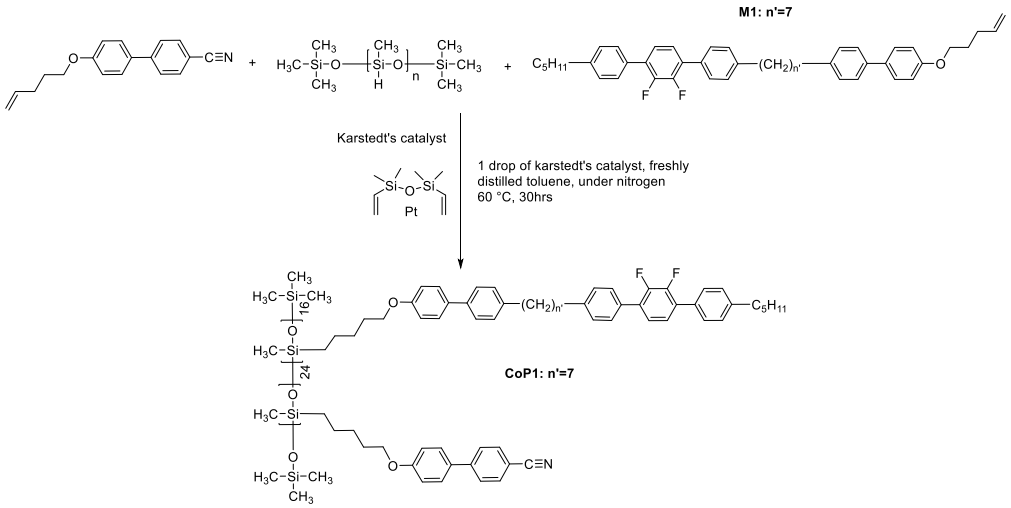
Yield: 0.031g, 25.6%.

^{1}HNMR (400 MHz, $CDCl_3$): δ 7.46 (t, 9H), 7.22 (s, 7H), 6.80 (s, 2H), δ 3.84 (s,2H), 2.62 (s, 8H), 1.33 (s, 17H), 1.27 (d, 18H), 0.97–0.76 (m, 13H), 0.23–0.02 (m, 48H) (as shown in Figure 3).

The calculation of the yield is listed in Figure S1.

2.7. Synthesis of the Copolymer (CoP1)

After the hydrosilylation reaction with poly(methylhydrosiloxane) and **M1** using Karstedt's catalyst, **CoP1** was obtained. The synthesis is described in detail below (see Scheme 4).



Scheme 4. Synthesis route of homopolymer **CoP 1**.

CoP1

The polymers were synthesized by the hydrosilylation of the monomer 4′-(pent-4-en-1-yloxy)-[1,1′-biphenyl]-4-carbonitrile (1.2 g, 4.56 mmol) and polymethylhydrosilane (Mn ≈ 1700~3200, 0.051 g, 0.85 mmol) using dry toluene as solvent with 2 drops of Karsted's catalyst (Pt ~2%) and stirred at 60 °C for 3 days while kept under an atmosphere of nitrogen. After the reaction was finished, further purification was carried out by repeated precipitation into methanol several times, and the product was dried under vacuum.

Isolated yield: 0.102 g, 21.2%.

^{1}HNMR (400 MHz, $CDCl_3$) solvent: δ 7.71–7.30 (m,6H), 6.84 (s, 2H), 3.86 (s, 2H), 1.75 (s, 2H), 1.45 (s, 4H), 0.57 (s, 2H), 0.07 (dd, J = 13.9, 8.0 Hz, 4H).

The calculation of the yield is listed in the Figure S1.

The GPC results indicate that the polydispersity is relatively narrow and broadly like that of the polymer backbone before the reaction, for the homopolymer and copolymer (see Table 1).

Table 1. GPC results of polymers.

Compound No	GPC Results			Weight Average DP Obtained by GPC	Average Molecular Weight of Repeating Units
	$\overline{Mw}$	$\overline{Mn}$	$\overline{Mw}/\overline{Mn}$	$\overline{Mw}/M_0$	
Polysiloxane backbone	830	663	1.3	13.8	60.1
HP1	21,494	15,441	1.4	29.4	730.4
PCN	28,848	14,212	2.0	89.3	323.1
CoP1 (**M1**: **MCN** = 1.2: 0.8)	22,720	12,778	1.8	40	567.5

3. Results and Discussion

3.1. DSC Studies

To investigate the phase behavior of materials, DSC measurements were used, and the data for the second cooling and heating curves are listed below (Table 2):

(a) Cr = crystalline; I = isotropic; N_x = unknown nematic phase; Sm_x = unknown smectic phase.
(b) Monotropic phases are shown in square brackets; enthalpies are shown in parentheses, unit (J/g).
(c) Peak width was measured as the difference between onset and offset temperatures (°C).

Table 2. Phase transition and phase transition enthalpies for monomer, pentamethyldisiloxane derivative and polymers.

Compound No	Spacer Length	Number of F Groups Attached	Transition Temperature °C (Using Onset and Offset of the Peaks), Measured by DSC at 10 °C/min, Enthalpies Unit (J/g)	Highest LC-I Temperature Peak Width
M1	5	2	Cr 87.5 N_{tb} 101.5 (10.1) N 113.0 (0.5) I	3.8
			I 114.2 (−0.5) N 102.5 (−10.2) N_{tb} 90.6 (−3.6) Sm_x 59 Cr	3.9
MCN	-	-	Cr 86.4 (93.7) I	-
			I 66.9 (−1.5) [N 49.3] Cr	1.5
PMDS 1	5	2	Cr 68.7 Sm_x 92.5 (1.8) SmA 110.5 (17.5) I	2.4
			I 108.6 (−17.7) SmA 90.4 (−1) Sm_x 45.3 Cr	2.5
HP1	5	2	Cr 107.1 N_x 182.9 (10.6) I	32.8
			I 174.1 (−10.4) N_x 106.8 Cr	29.6
PCN	5	0	S_A 164.9 (5.2) I	9.5
			I 166.6 (−5.3) S_A	4.9
CoP1 (**M1**: **MCN** = 1.2: 0.8)	5	2	N 141.39 (7.0) I	34.5
			I 148.3 (−5.9) N	38.6

Melting point and isotropisationtemperature are both measured as the onset temperature of the 2nd heating and cooling curves as measured by DSC. The melting points for polymer **PCN** and **CoP1** cannot be determined as below the room temperature.

To facilitate the comparison, the thermal properties of monomer **M1**, the pentamethydisiloxane **PMDS1** and polymers are given in Table 2. After polymerization, both melting points and isotropization temperature for the polymer increase when compared with the related monomer and the pentamethydisiloxane **PMDS1**. For the pentamethydisiloxane, the transition temperature and the liquid crystal phase behaviors can often provide very useful information for the prediction of the related homopolymers [22–24]. All the phase transitions are reduced for the pentamethydisiloxane **PMDS1** when compared with the related monomer. Homopolymer 1 (**HP1**) shows crystallization without a glass transition. A route to eliminate the crystallization is through the introduction of another mesogenic monomer or even non-mesogenic units, to separate the liquid crystal side chains. For copolymer (**CoP1**), both crystallization tendencies and melting points are eliminated on the second heating and cooling curve of the DSC, and the liquid crystal phase is stable at room temperature. The isotropization temperature decreases for the copolymer, compared with homopolymer. It is noteworthy that not only can copolymerization help to eliminate the crystallization, but it can also help to stabilize the liquid crystal phase at room temperature. Based on the transition temperatures of **HP1** and **CoP1** (Table 2), the crystalline tendencies are eliminated in the copolymer because the incorporation of the short spacer length of the monomer 4′-(pent-4-en-1-yloxy)-[1,1′-biphenyl]-4-carbonitrile has broken the π-π interactions of the phenyl rings of the long side chains. In addition, due to the flexibility of the polymer backbones, the glass transition temperature is lower than room temperature.

An interesting and important feature is the width of the N-Iso transition on linking **M1** either to a pentamethyldisiloxane end group or to the polysiloxane main chain. **M1** is characterized by a transition width of 3.8–3.9 °C, somewhat wider than the monomeric material **MCN** known in the literature but in line with results reported for other dimesogenic dimers with lateral fluoro groups. Linking **MCN** to a polysiloxane main chain results in **PCN**, as well as a widening of the transition interval and an increase in the

enthalpy, in line with the original reports [21,22]. Typically, the widening of transitions on attachment to polymers is linked to kinetic effects; molecular mobility is decreased due to increased viscosity, but even more so, it is linked to the influence of the polydispersity of the main chain. Polymer chains of differing lengths exhibit different transition temperatures. A polydisperse sample is thus an ensemble of a series of systems, transitioning at different temperatures, and, together with the ensuing biphasic regions associated with first-order phase transitions, is the cause of widening the transition intervals. Attachment of **M1** to a pentamethyldisiloxane end group narrows the transition somewhat to 2.4–2.5 °C when compared to **M1** with the vinylic end group of (3.8–3.9 °C), but the transition enthalpy increases dramatically to 17.5–17.7 J/g, very high for a liquid crystal to isotropic transition. This is indicative of a major order–disorder transformation. It suggests also that a different LC phase may have formed as the highest stable LC state. The attachment to the polysiloxane main chain has an equally dramatic effect. The transition to the monotropic low-temperature smectic phase of **M1** is lost, and the transition enthalpy is reduced to 10.4–10.6 J/g when compared to the pentamethyldisiloxane derivative **PMDS1**, indicative of a lower ordering. However, the transition interval is enormous; it reaches 29.6–32.8 °C, depending on whether the values are collected on heating or cooling. This suggests that multiple processes take place. For **M1**, the nematic phase range is ~12 °C, and the N_{tb} phase has a range of about 30 °C. The extreme widening of the transition in **HP1** would thus be explainable by a combination of the biphasic behavior observed already in mixtures of dimers. Additional phase transition peaks seem to appear in DSC experiments but are related to the effects of the end points of the biphasic regions of the phase diagram [25]. For the polymer, additionally, an overlap of the phase transitions of polymers of different chain lengths and transitions between different phases such as the N and the N_{tb} phase play a role. In other words, when on cooling, some of the polymer chains in this ensemble still undergo an Iso to N transition, others are already on the way to the N to N_{tb} transition. This broadens the transition range to the extreme. This view is supported by the results for **CoP1**. Even more molecular complexity is introduced; the range of the transition interval increases marginally to 34.6–38.6 °C, but the transition enthalpy associated with the loss of order is broadly similar to that for **PCN** and much smaller than observed for **HP1**. This confirms the argument that for **HP1**, a broad and flat peak masks multiple transitions in the polymer. However, as only one transition was detectable by DSC, the term N_x is used for the LC phase in Table 2.

3.2. POM Studies

The liquid crystal defect textures of **M1**, obtained from POM are shown below (see Figure 4a–f). The material forms a nematic phase at 114 °C, the texture of the nematic phase is shown in Figure 4a, and a further phase transition takes place at 103 °C (shown in Figure 4b), close to the DSC measured value of 102.5 °C (the DSC scan was recorded at the rate of 10 °C/min). The texture changes indicate a transition from the nematic phase (see Figure 4a) to the twist-bend nematic phase (Figure 4c). The twist-bend nematic phase texture does not change under slight shearing (Figure 4d). After being sheared at 80 °C, the texture does not change much but flows very slowly due to high viscosity (Figure 4e). If the sample is sheared more vigorously at 95 °C, a texture change occurs, and only a homotropic texture is observed (Figure 4f). Texture changes associated with the phase transition at 89.9 °C could not be identified that clearly under POM; however, a more ordered smectic phase had formed noticeably in shearing experiments where a very high viscosity was noticed. It was also found that the cooling rate strongly influences the POM textures. When cooling at a high rate of 10 °C/min, the texture shows no focal conic type of shape defects (Figure 5a). Reducing the cooling rate to 3 °C/min induces small focal conic features (Figure 5b), further reducing the cooling rate to 0.1 °C/min, results in larger focal conic domains (see Figure 5c).

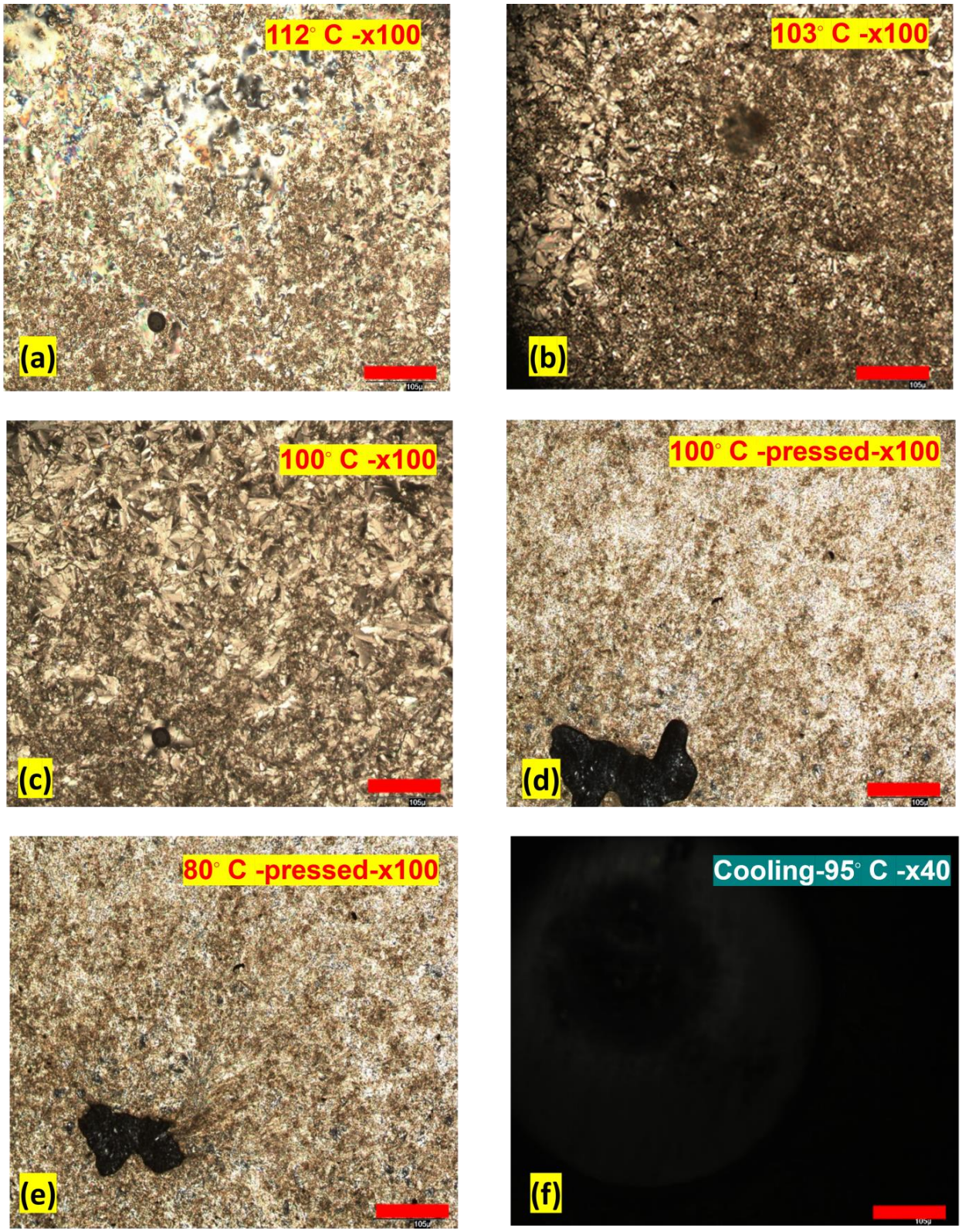


Figure 4. POM of monomer **M1**; the scale bar is 105 µm for magnification ×100; the scale bar is 42 µm for magnification ×40. (**a**) Nematic phase at 112 °C; (**b**) phase transition at 103 °C (top left is in the N_{tb} phase, while bottom right is in the N phase); (**c**) N_{tb} phase at 100 °C; (**d**) N_{tb} phase at 100 °C after shearing; (**e**) phase texture under gentle shearing at 80 °C; (**f**) homeotropic texture after shearing at 95 °C, magnification ×40.

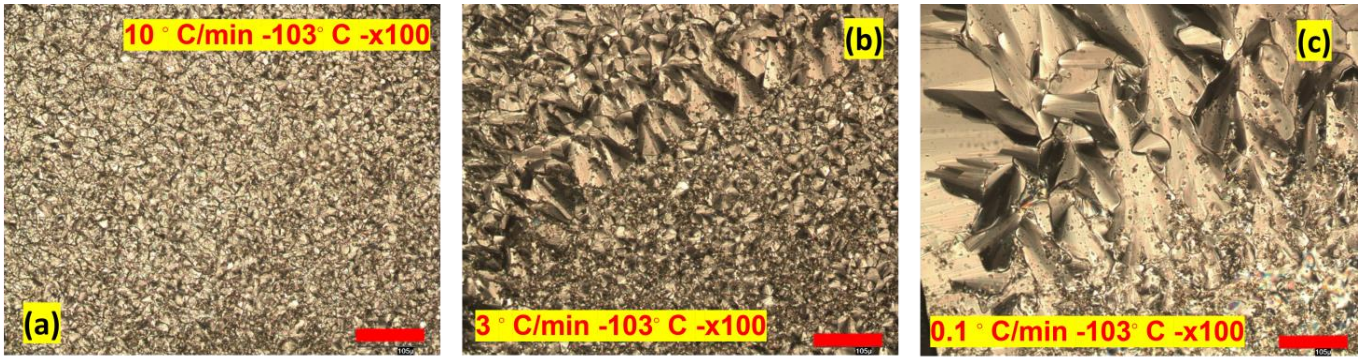


Figure 5. Textures measured by POM of **M1** at 103 °C at different cooling rates. The scale bar is 105 µm for magnification ×100. Top left is the N_{tb} phase, and bottom right is the nematic phase. (**a**) Cooling rate at 10 °C/min, 103 °C; (**b**) cooling rate at 3 °C/min, 103 °C; (**c**) cooling rate at 0.1 °C/min, 103 °C.

It is interesting to analyze the liquid crystal phase formed by the pentamethydisiloxane functionalized monomer **M1** that exhibits N_{tb} phase behavior. As shown in Figure 6a, **PMDS1** exhibits an SmA phase that emerges from the isotropic state with atypical bãtonet defect texture [26]. The bãtonets merge to form the smectic phase texture (see Figure 6b). As the temperature is reduced, the bãtonets grow into mini-focal-conic domains. As the end group is a widely reported pentamethydisolane group, this is not surprising, as this type of siloxane end group can produce nano-segregation to form smectic phase behavior [27]. The short siloxane group disturbs the formation of the heliconical structure and favors layer formation. This results in an SmA phase.

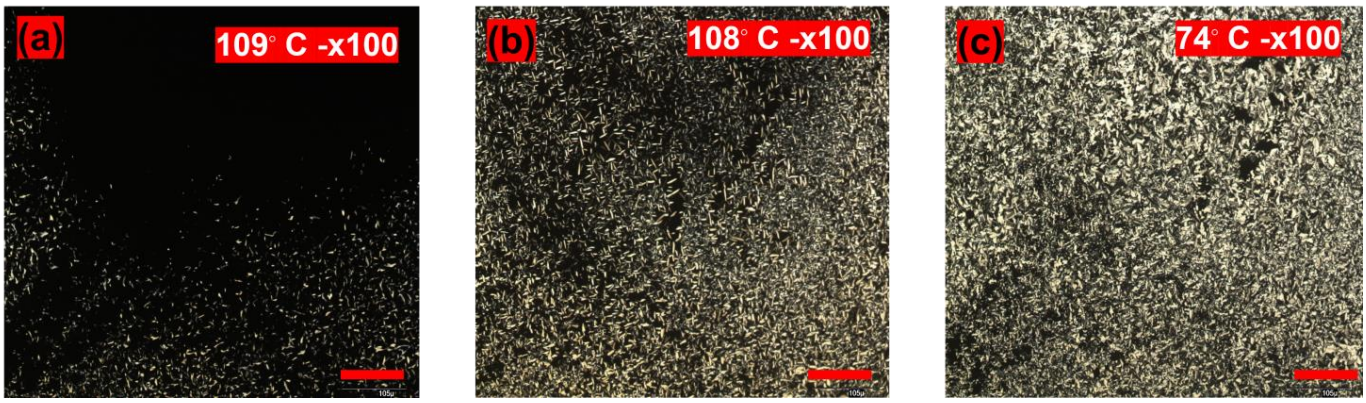


Figure 6. POM of pentamethydisiloxane derivative **PMDS1**; the scale bar is 105 µm for magnification ×100. (**a**) A smectic phase emerges from the isotropic state. Bãtonet shapes at 109 °C (**b**) SmA phase at 108 °C and (**c**) SmX phase at 74 °C.

To identify the phase texture of the **HP1**, contact preparations of **DTC5C7** (see Figure 7) with homopolymer 1 (**HP1**) were carried out and monitored by POM. **DTC5C7** was chosen as a contact compound for **HP1**. One reason is that **DTC5C7** has broadly similar transition temperatures when compared to **HP1**; the other reason is that its N_{tb} phase transition temperature is located within the phase transition range of **HP1**. This makes it a good tool for identifying the existence of a N_{tb} phase in **HP1**. The results can be found in Figure 8 and Supporting Information Figure S1. On the left-hand side, **DTC5C7** is shown in the micrographs, while on the right-hand side, the defect textures of **HP1** can be seen. From the Supporting Information Figure S1a,b, it can be seen that as the temperature is reduced to 120 °C, the texture changes from the Nto the N_{tb} phase. After annealing the polymer for 1 day, the two mesophases' textures began to merge (see Supporting Information Figure S1c).

Further annealing for 2 days made the textures clearer, the whole area of **DTC5C7** and **HP1** completely merged and exhibited the same texture as shown in Supporting Information Figure S1f. Figure 8a,b, show the coalescence of both compounds at 120 °C over a wider viewing field. This result needs further confirmation; the current data, however, reveal that the N_{tb} phase of **DTC5C7** and the unknown nematic phase, provisionally identified as N_x of **HP1**, mix fully. As both molecules are structurally very similar, this suggests that the N_x phase of the **HP1** is a N_{tb} phase. This would be the first example of a N_{tb} found in a side-chain polymer.

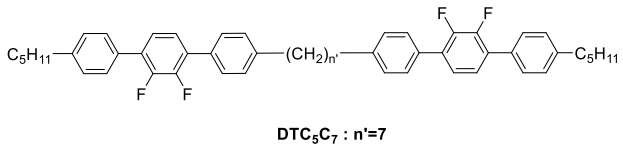


Figure 7. Structure of DTC5C7.

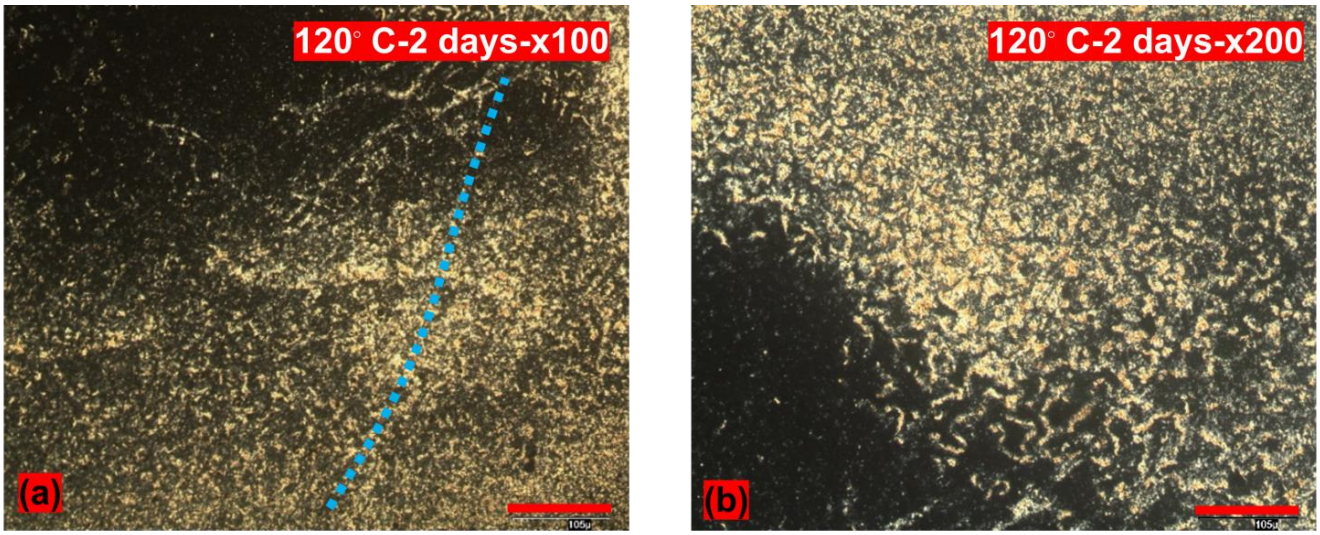


Figure 8. Textures of the contact preparation of **HP1** with **DTC5C7**, displayed by polarized optical microscopy. The scale bar is 105 µm for magnification ×100; the scale bar is 210 µm for magnification ×200. The sample of **DTC5C7** is located on the left side of the slides, the **HP1** is located on the right side of the slides, and the blue dash line indicates the initial separation line of the binary mixtures: (**a**) texture at 120 °C after annealing for 2 days, magnification ×100, both sides completely merge; (**b**) texture at 120 °C after annealing for 2 days, magnification ×200, both sides completely merge, and the N_{tb} phase texture is clear to view.

3.3. X-ray Powder Diffraction

The results of X-ray powder diffraction analysis for the copolymer that exhibits one liquid crystal phase, which is stable at room temperature, are discussed. The X-ray powder diffraction was collected to gain more information on the phase structure (see Figure 9 and Table 3). The X-ray powder diffraction pattern is dominated by a wide-angle intensity at $2\theta = 19.8°$ (d = 4.49 Å). This is related to the lateral packing of the fluidic mesogens in the liquid crystal state. The shoulder-like peak at $2\theta = 12.3°$ (d = 7.2 Å) is often found for siloxane polymers. The small angle peak at $2\theta = 4.25°$ (d = 20.8 Å) is typical for N_{tb} and N materials and is simply associated with the electron densities of the mesogenic units which are only orientationally ordered but do not have positional ordering [17]. This confirms that the overall phase structure is that of a nematic-like phase.

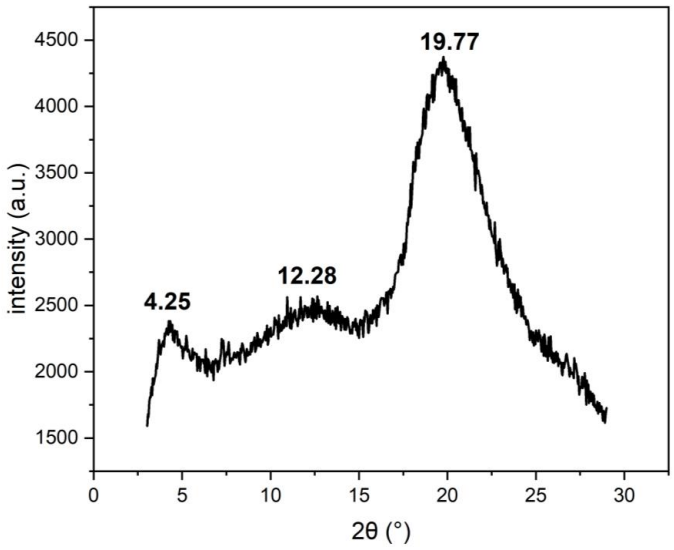


Figure 9. Plot of 2θ against intensity of the X-ray powder diffraction patterns at room temperature of copolymer 1 (**CoP1**).

Table 3. Summary of X-ray powder diffraction data of copolymer 1 (**CoP1**) at room temperature.

2θ (°)	d-Value (Å)
4.25	20.78
12.28	7.20
19.77	4.49

3.4. Phase Diagram

As it was found to be difficult to identify the phase structure of the monomer unambiguously, an exploratory phase diagram with defined mixtures was constructed, following the results of DSC experiments. The phase diagram of binary mixtures of **CBC9CB**. the structure is shown in Figure 10, and monomer **M1** was constructed to identify the phase transitions of the N_{tb} phase.

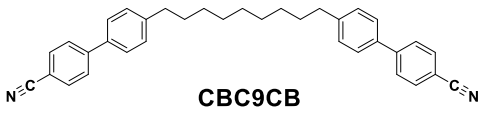


Figure 10. Structure of **CBC9CB** [28].

CBC9CB was chosen as a contact compound for monomer **M1**. One reason is that it has a broad temperature range of the N_{tb} phase; the other reason is that its N_{tb} phase transition temperature is broadly similar to the phase transitions of **M1**. This makes it a good indicator of the existence of a N_{tb} phase in **M1** [28].

The exploratory phase diagram for the mixtures of **CBC9CB** and monomer **M1** shows the results from the second cooling DSC run (Figure 11a). The transition temperature from the nematic to the isotropic decreases somewhat linearly with an increasing amount of **M1**. Progressing from pure **CBC9CB** to pure monomer **M1**, the nematic phase range firstly becomes wider, then is reduced to the narrowest area at 50 wt% and finally grows slightly on the side of the monomer **M1**. The N_{tb} region for both pure compounds is wider until approaching ~50 wt%, which exhibits the narrowest range. Interestingly, for the mixtures, the N_{tb} phase is enantiotropic, independent of the composition change. For 25%wt and 75%wt mixtures, the N_{tb} phase is stable at room temperature, whereas for 50 wt%, the N_{tb}

phase is only stable over a small temperature range and finally changes to a smectic phase whose structure is still to be determined.

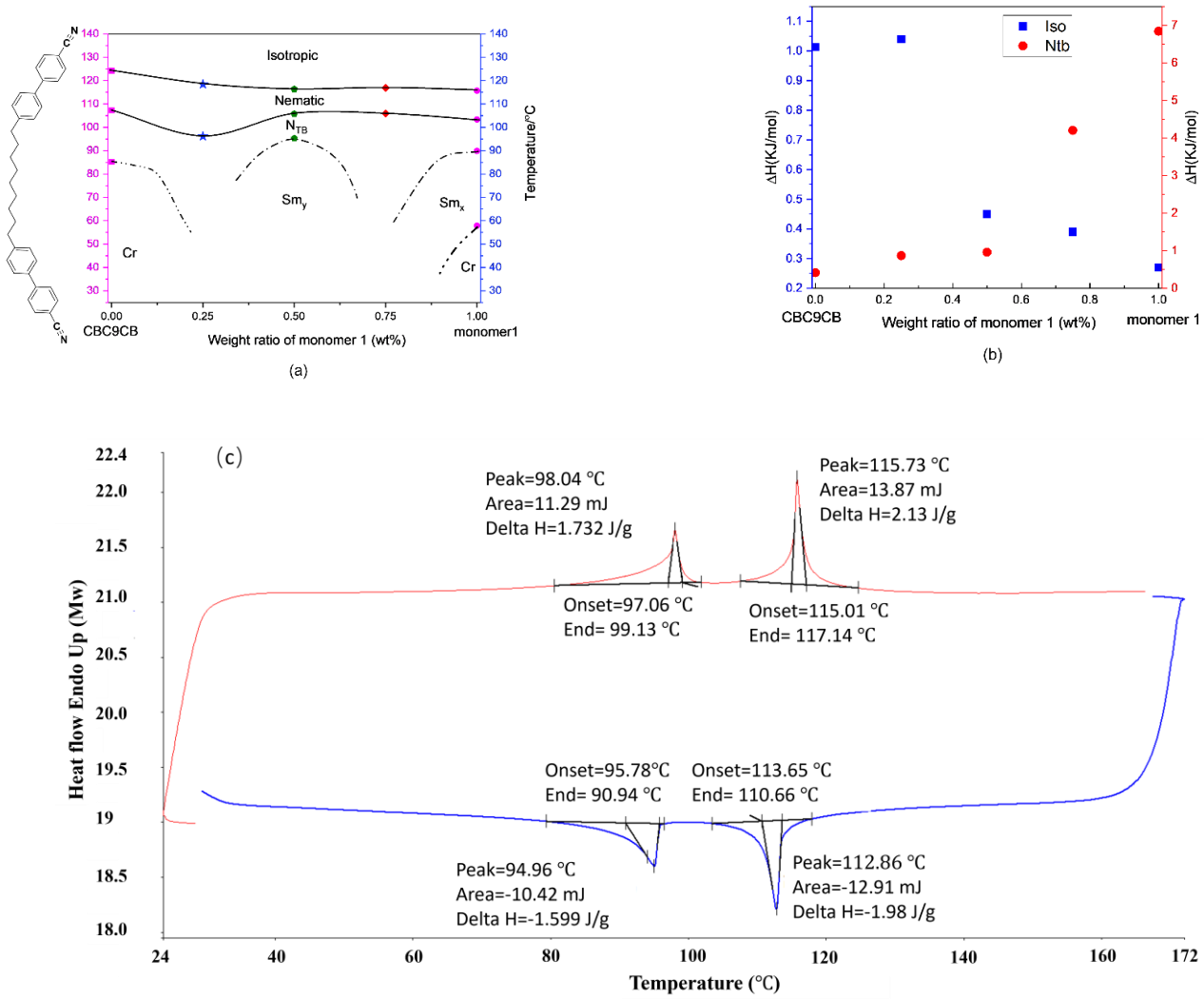


Figure 11. (**a**) Temperature concentration phase diagrams for the **CBC9CB-M1** binary mixtures. Closed colorful symbols are used to denote the transition temperatures taken from the second cooling DSC run. Dash lines represent potential transitions unresolved by the DSC experiments. (**b**) Temerarutes in (°C), instrument heating data in mJ, enthalpy values (ΔH) in J/g from the second cooling run of DSC as a function of concentration of monomer **M1**, for the Iso-N and N-N_{tb} phase of the **CBC9CB-M1** binary mixtures. Red closed circles represent the N-N_{tb} enthalpy changes, while blue square represents the Iso-N enthalpies. (**c**) Second heating and cooling curve at 10 °C/min result of a 25 wt% **M1** and 75 wt% **CBC9CB**.

Figure 11b shows the enthalpy values of the mixtures as a function of the concentration of monomer **M1**; the enthalpies are associated with the Iso-N and N-N_{tb} transition and are based on the measurements obtained from the second cooling runs of the DSC scans. They are plotted as a function of the concentration of monomer **M1** in **CBC9CB** binary mixtures. The enthalpy values for the Iso-N transition exhibit a substantial decrease with an increasing molar fraction of the monomer **M1**. The values of the transition enthalpy of pure **CBC9CB** of 1.0 KJ/mol to 0.3 KJ/mol for pure monomer **M1** are quite different. It is noted that the **CBCnCB** series exhibit different enthalpy values for the N-Iso transition compared to dimers containing fluoro groups in the mesogenic units [29]. The enthalpy values for the N-N_{tb} transition display a dramatic increase with an increasing concentration of monomer **M1**. With the value from the transition enthalpy of pure **CBC9CB** of 0.4 KJ/mol

increasing to 6.8 KJ/mol for pure monomer **M1**, this is almost seventeen times larger in value. Figure 11c shows the DSC results of one of the mixtures 25 wt% **M1**–75 wt% **CBC9CB** as an example. In addition to the wide melting transitions, the exothermic peak related to the crystallization temperature was not observed by DSC, because the system forms a glassy liquid crystal state above 30 °C. Similar results were observed by DSC on the second heating and cooling curves for all the other mixtures.

3.5. Polysiloxanes

For homopolymer 1 (**HP1**), there is only one liquid crystal phase recorded by DSC. However, it is noted that the peak is broad and unresolved, and thus a phase transition between the nematic and the N_{tb} phase might be obscured or simply not measurable due to a biphasic region. From Figure 8, it can be provisionally deduced that this is a N_{tb} phase since there is no boundary or miscibility gap between the binary mixtures of **DTC5C7** and **HP1** in the N_{tb} phase. POM pictures for **HP1** depicted in Supporting Information Figure S2 show that this liquid crystal texture remains the same until crystallization at 107.9 °C.

POM pictures for the copolymer **CoP1** are also shown in Figure 12. Schlieren textures are clearer at temperatures close to isotropization temperature. Crystallization peaks were not traced by DSC, because the polymer remains in the liquid crystal phase at room temperature. This was already evidenced by X-ray powder diffraction experiments measured at room temperature (Figure 9). Recording pictures at higher magnification shows that branches between long rope-like features occur (see Figure 12e,f), and long annealing times reveal an oily streak-like texture which can often be observed for N_{tb}-forming materials. This might be interpreted as a variation of the rope texture that is found often in twist-bend systems.

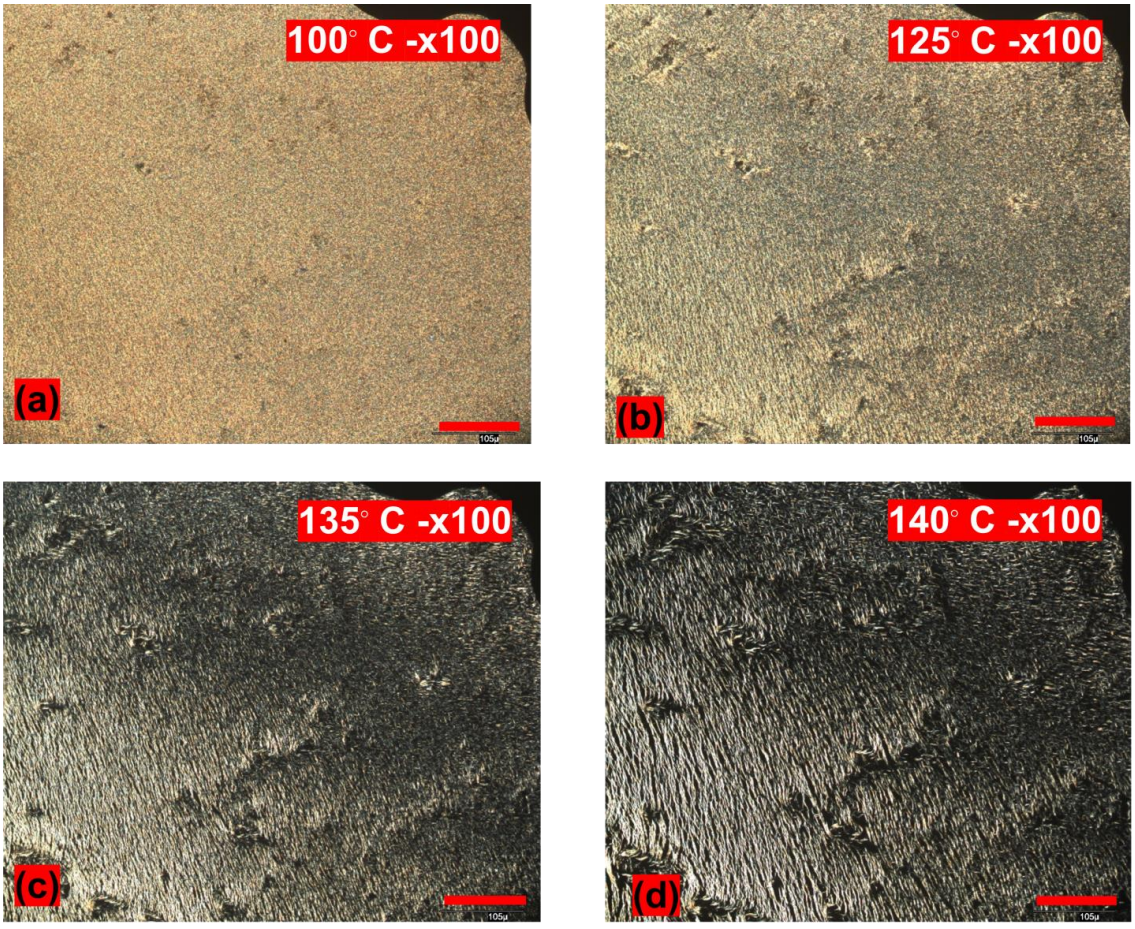


Figure 12. *Cont.*

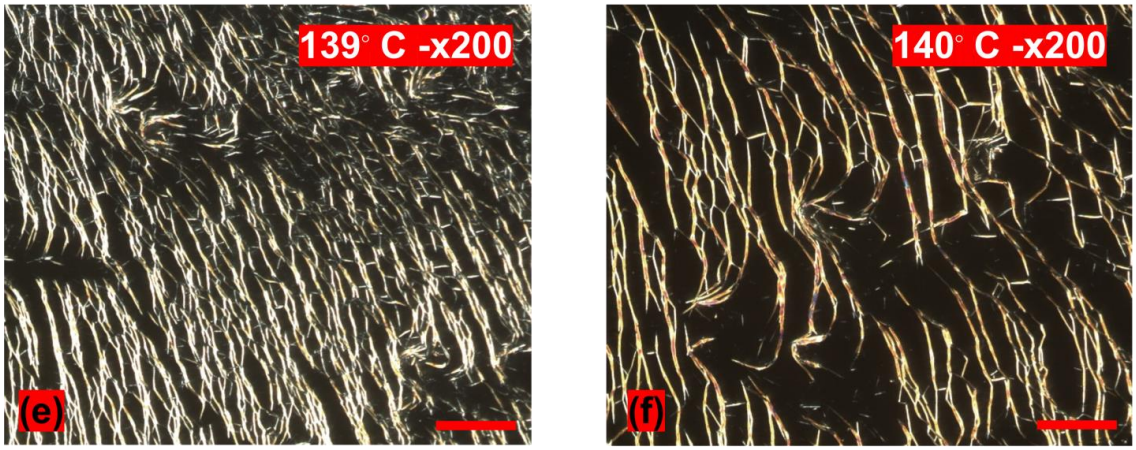


Figure 12. Polarized optical microscopy displayed by flow-filled slide of copolymer **CoP1**. The scale bar is 105 μm for magnification °100; the scale bar is 210 μm for magnification °200. (**a**) N_x phase at 100 °C; (**b**) N_x phase at 125 °C; (**c**) N_x phase at 135 °C; (**d**) N_x phase at 140 °C; (**e**) N_{tb} phase in a schlieren texture at 139 °C, magnification 200; (**f**) N_x phase in schielren texture at 140 °C, magnification °200.

The thermal behavior of a comparative mixture of **M1** and **MCN** (molar ratio of 1.2:0.8, the same as in **CoP1**) was studied by POM. The POM data, for that mixture, show a nematic to smectic A phase transition on cooling at 105 °C (see Figure 13a–c). When these two monomers are linked to the polymer backbone, the smectic A phase is suppressed in **CoP1**, and the nematic phase remains. As observed for **HP1**, the phase transition range as measured by DSC is extremely wide, possibly masking a N-N_{tb} transition; this would be in line with POM observations. However, in the absence of more detailed studies, potentially with more complex behavior as a copolymer involved, the phase is provisionally identified as N_x.

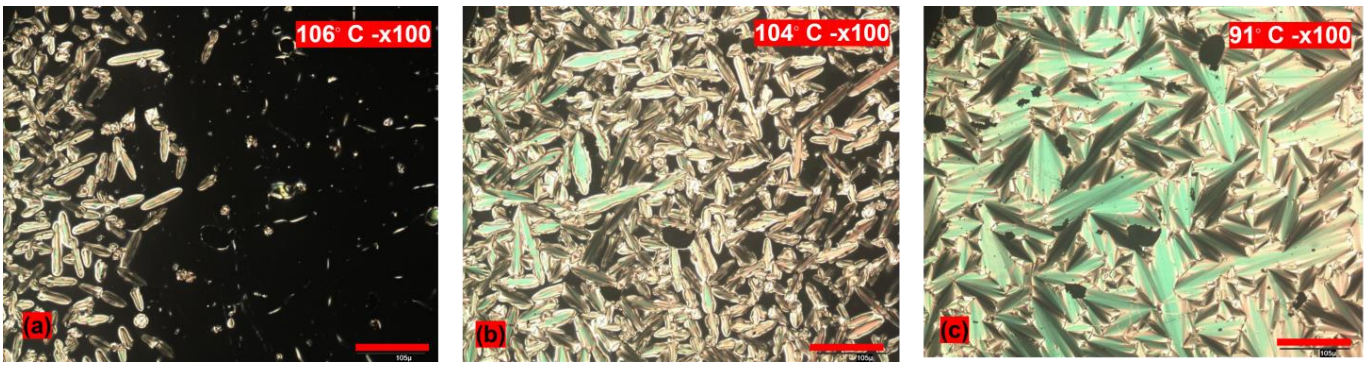


Figure 13. Polarized optical microscopy of mixture of **M1**:**MCN**; molar ratio = 1.2:0.8. The scale bar is 105 μm for magnification °100. (**a**) Phase transition from a nematic phase with a homeotropic orientation to the SmA phase at 106 °C; (**b**) SmA phase at 104 °C; (**c**) SmA phase at 91 °C.

4. Conclusions

A new vinylic dimesogenic monomer showing the N_{tb} phase was synthesized. Current synthetic methods were improved for achieving material containing an isomer-free olefin group. A pentamethyldisiloxane group was attached to this monomer, resulting in the SmA LC phase behavior of the ensuing material. Linking the monomer to a siloxane main chain results in a polymer, forming nematic phase behavior with an extremely wide transition range. Detailed studies with the N_{tb}-phase-forming dimer **DTC5C7** show full miscibility of the dimer and the new LC polymer in all LC phases, suggesting that the side-chain LC polymer forms a N_{tb} phase as a low-temperature nematic phase. Copolymerizing the

monomer with a cyanobiphenyl-based monomer allows us to tune the glass transition, prevent crystallization and tune the phase behavior further to a nematic phase behavior at room temperature.

Supplementary Materials: The following supporting information can be downloaded at: https://www.mdpi.com/article/10.3390/cryst13121614/s1; S1 isolated polymer yield calculations; S2. POM textures.

Author Contributions: W.J. synthesized and chemically analyzed the compounds with input from G.H.M. G.H.M. designed the project. W.J. and G.H.M. wrote the manuscript together. All authors have read and agreed to the published version of the manuscript.

Funding: The project was supported by the CSC (Chinese Scholarship Council) and the University of Hull as part of a doctoral programme. W.J. thanks also the Henry Lester Trust, the Great Britain-China Educational Trust and the British Federation of Women Graduates for support for the living expenses during the Ph.D. program. We acknowledge the support by Diamond Light Sources UK (SM33389).

Data Availability Statement: The data presented in this study are available in within this manuscript and the Supporting Information.

Acknowledgments: We want to say thank you to Robert Lewis, Tim Prior, Timothy Dunstan, Chris Welch, Dean Moore and Sean Moore from the University of Hull Chemistry Department for their help in the collection of DSC, elemental analysis, GPC and X-ray powder diffraction data.

Conflicts of Interest: The authors declare no conflict of interest.

References

1. Finkelmann, H.; Happ, M.; Portugal, M.; Ringsdorf, H. Liquid crystalline polymers with biphenyl-moieties as mesogenic group. *Die Makromol. Chem. Macromol. Chem. Phys.* **1978**, *179*, 2541–2544. [CrossRef]
2. Finkelmann, H.; Ringsdorf, H.; Wendorff, J.H. Model considerations and examples of enantiotropic liquid crystalline polymers. Polyreactions in ordered systems, 14. *Die Makromol. Chem. Macromol. Chem. Phys.* **1978**, *179*, 273–276. [CrossRef]
3. Finkelmann, H.; Koldehoff, J.; Ringsdorf, H. Synthesis and Characterization of Liquid-Crystalline Polymers with Cholesteric Phase. *Angew. Chem. Int. Ed. Engl.* **1978**, *17*, 935–936. [CrossRef]
4. Finkelmann, H.; Day, D. Structure of mesomorphic polymer phases. *Die Makromol. Chem. Macromol. Chem. Phys.* **1979**, *180*, 2269–2274. [CrossRef]
5. Finkelmann, H.; Rehage, G. Investigations on liquid crystalline polysiloxanes, 2. Optical properties of cholesteric phases and influence of the flexible spacer on the mobility of the mesogenic groups. *Die Makromol. Chem. Rapid Commun.* **1980**, *1*, 733–740. [CrossRef]
6. Finkelmann, H.; Rehage, G. Investigations on liquid crystalline polysiloxanes, 1. Synthesis and characterization of linear polymers. *Die Makromol. Chem. Rapid Commun.* **1980**, *1*, 31–34. [CrossRef]
7. Milano, J.C.; Robert, J.M.; Vernet, J.L.; Gallot, B. The thioether spacer in liquid crystalline polysiloxanes with cyano-and nitrobiphenyl mesogens. *Macromol. Chem. Phys.* **1999**, *200*, 1580–1586. [CrossRef]
8. Jeng, G.P.C.; Kuo, J.F.; Chen, C.Y. Synthesis and mesomorphic behavior of terminally carboxyl oligo (ethylene oxide) monomethyl ethers-substituted side chain liquid crystalline polysiloxanes. I. *J. Appl. Polym. Sci.* **1993**, *47*, 697–706. [CrossRef]
9. Gray, G.W.; Hill, J.S.; Lacey, D. Synthesis and properties of some liquid crystal polysiloxanes with laterally or terminally attached side chains. *Mol. Cryst. Liq. Cryst.* **1991**, *197*, 43–55. [CrossRef]
10. Day, G.M.; Kim, H.-J.; Jackson, W.R.; Simon, G.P. Synthesis and characterization of novel chiral liquid crystalline polysiloxanes. *Acta Polym.* **1999**, *50*, 96–104. [CrossRef]
11. Hsu, C.S.; Lu, Y.H. Synthesis and characterization of side-chain liquid crystalline polysiloxanes containing 4-alkanyloxyphenyl trans-4-alkylcyclohexanoate side groups. *J. Polym. Sci. Part A Polym. Chem.* **1991**, *29*, 977–986. [CrossRef]
12. Richard, H.; Mauzac, M.; Sigaud, G.; Achard, M.; Hardouin, F. Liquid crystal side chain polysiloxanes containing various proportions of non-mesogenic units. *Liq. Cryst.* **1991**, *9*, 679–689. [CrossRef]
13. Kawashima, Y.; Nozaki, K.; Hiyama, T.; Yoshio, M.; Kanie, K.; Kato, T. Liquid-crystalline stereoregular polyketone prepared from a mesogenic vinylarene and carbon monoxide. *J. Polym. Sci. Part A Polym. Chem.* **2003**, *41*, 3556–3563. [CrossRef]
14. Gu, H.D.; Chen, L.; Yan, J.X. Effect of chiral isosorbide groups on mesomorphic properties of side-chain liquid-crystalline polysiloxanes. *Liq. Cryst.* **2009**, *36*, 1319–1327. [CrossRef]
15. Huang, H.; Cong, Y.; Lin, Z.; Zhang, B. Synthesis and properties of side-chain liquid crystalline polymers grafted with chiral dimers containing cholesteryl groups. *Liq. Cryst.* **2020**, *47*, 723–736. [CrossRef]
16. Saha, R.; Babakhanova, G.; Parsouzi, Z.; Rajabi, M.; Gyawali, P.; Welch, C.; Mehl, G.H.; Gleeson, J.; Lavrentovich, O.D.; Sprunt, S. Oligomeric odd–even effect in liquid crystals. *Mater. Horiz.* **2019**, *6*, 1905–1912. [CrossRef]

17. Ahmed, Z.; Welch, C.; Mehl, G.H. The design and investigation of the self-assembly of dimers with two nematic phases. *RSC Adv.* **2015**, *5*, 93513–93521. [CrossRef]
18. Johnson, C.R.; Braun, M.P. A two-step, three-component synthesis of PGE1: Utilization of. alpha.-iodo enones in Pd (0)-catalyzed cross-couplings of organoboranes. *J. Am. Chem. Soc.* **1993**, *115*, 11014–11015. [CrossRef]
19. Mano, J.F.; Correia, N.T.; Moura Ramos, J.J.; Fernandes, A.C. A thermally stimulated discharge currents study of the molecular motions in two polysiloxane side-chain liquid crystalline polymers. *J. Polym. Sci. Part B Polym. Phys.* **1995**, *33*, 269–277. [CrossRef]
20. McArdle, C.B. *Side Chain Liquid Crystal Polymers*; Springer Science & Business Media: Berlin/Heidelberg, Germany, 1990.
21. Gemmell, P.; Gray, G.W.; Lacey, D. Effects of molecular structure on the properties of terminally cyano-substituted side chain liquid crystalline polysiloxanes. *Mol. Cryst. Liq. Cryst.* **1985**, *122*, 205–218. [CrossRef]
22. Stevens, H.; Rehage, G.; Finkelmann, H. Phase transformations of liquid crystalline side-chain oligomers. *Macromolecules* **1984**, *17*, 851–856. [CrossRef]
23. Finkelmann, H. Liquid crystalline side-chain polymers. Philosophical Transactions of the Royal Society of London. *Ser. A Math. Phys. Sci.* **1983**, *309*, 105–114.
24. Shibaev, V.; Plate, N. Synthesis and structure of liquid-crystalline side-chain polymers. *Pure Appl. Chem.* **1985**, *57*, 1589–1602. [CrossRef]
25. Ramou, E.; Ahmed, Z.; Welch, C.; Karahaliou, P.; Mehl, G.H. The stabilisation of the Nx phase in mixtures. *Soft Matter* **2016**, *12*, 888–899. [CrossRef]
26. Dierking, I. *Textures of Liquid Crystals*; John Wiley & Sons: Hoboken, NJ, USA, 2003.
27. Newton, J.; Coles, H.; Hodge, P.; Hannington, J. Synthesis and properties of low-molar-mass liquid-crystalline siloxane derivatives. *J. Mater. Chem.* **1994**, *4*, 869–874. [CrossRef]
28. Paterson, D.A.; Abberley, J.P.; Harrison, W.T.; Storey, J.M.; Imrie, C.T. Cyanobiphenyl-based liquid crystal dimers and the twist-bend nematic phase. *Liq. Cryst.* **2017**, *44*, 127–146. [CrossRef]
29. Stevenson, W.D.; Zou, H.X.; Zeng, X.B.; Welch, C.; Ungar, G.; Mehl, G.H. Dynamic calorimetry and XRD studies of the nematic and twist-bend nematic phase transitions in a series of dimers with increasing spacer length. *Phys. Chem. Chem. Phys.* **2018**, *20*, 25268–25274. [CrossRef]

Disclaimer/Publisher's Note: The statements, opinions and data contained in all publications are solely those of the individual author(s) and contributor(s) and not of MDPI and/or the editor(s). MDPI and/or the editor(s) disclaim responsibility for any injury to people or property resulting from any ideas, methods, instructions or products referred to in the content.